
Environmental Change Detection: Toward a Practical Task of Scene Change Detection

Kyusik Cho¹ Suhan Woo¹ Hongje Seong^{2*} Euntai Kim^{1*}
¹Yonsei University ²University of Seoul
{ks.cho, wsh112, etkim}@yonsei.ac.kr, hjseong@uos.ac.kr

Abstract

Humans do not memorize everything. Thus, humans recognize scene changes by exploring the past images. However, available past (*i.e.*, reference) images typically represent nearby viewpoints of the present (*i.e.*, query) scene, rather than the identical view. Despite this practical limitation, conventional Scene Change Detection (SCD) has been formalized under an idealized setting in which reference images with matching viewpoints are available for every query. In this paper, we push this problem toward a practical task and introduce Environmental Change Detection (ECD). A key aspect of ECD is to avoid unrealistically aligned query-reference pairs and rely solely on environmental cues. Inspired by real-world practices, we provide these cues through a large-scale database of uncurated images. To address this new task, we propose a novel framework that jointly understands spatial environments and detects changes. The main idea is that matching at the same spatial locations between a query and a reference may lead to a suboptimal solution due to viewpoint misalignment and limited field-of-view (FOV) coverage. We deal with this limitation by leveraging multiple reference candidates and aggregating semantically rich representations for change detection. We evaluate our framework on three standard benchmark sets reconstructed for ECD, and significantly outperform a naive combination of state-of-the-art methods while achieving comparable performance to the oracle setting. The code will be released upon acceptance.

1 Introduction

Change detection in images is a fundamental problem in computer vision. This problem has primarily been advanced through Scene Change Detection (SCD), which identifies differences between a reference image and a query image captured at distinct times. SCD has attracted increasing attention due to its potential in a wide range of practical applications, such as urban scene analysis [1, 2, 3], disaster damage assessment [4, 5], anomaly detection [6], and warehouse management [7, 8].

Despite its significance, SCD has limited applicability in real-world scenarios. We attribute this limitation to two unrealistic assumptions: (1) every query image is paired with a reference image, and (2) each query-reference pair is captured from the same location with an identical viewpoint. For example, VL-CMU-CD [1], one of the representative datasets in the SCD community, collects query-reference pairs and synthetically distorts the reference images to align with the viewpoint of the query. Conventional SCD approaches [9, 10] are developed with these datasets and detect changes through matching at corresponding spatial locations between a reference and a query. As a result, a minor misalignment may lead to failure in SCD. To overcome this problem, recent advances try to reduce reliance on the query-reference alignment (*i.e.*, the second assumption). SimSac [8] assumes coarsely aligned query-reference pairs and addresses minor misalignments via optical flow. RSCD [11] avoids pixel-wise direct matching and instead employs a cross-attention to consider

*Corresponding authors.

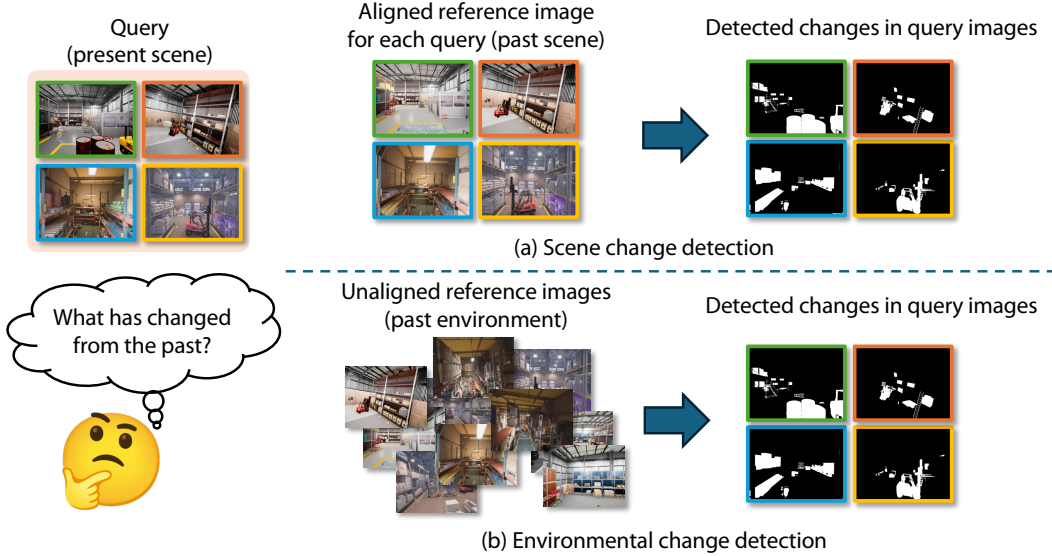


Figure 1: **Comparison between the problem settings of SCD and ECD.** In the conventional SCD setting, each query image is provided with its corresponding reference image as a predefined pair. In contrast, ECD considers a more challenging scenario where query-reference pair are unknown. ECD just provides a database of unaligned reference images. Furthermore, ECD does not guarantee the presence of a perfectly matched pair within the database.

misaligned pixels. Nevertheless, these approaches still rely on the availability of query-reference pairs (*i.e.*, the first assumption) and require coarse alignment (*i.e.*, a relaxed form of the second assumption).

To address these limitations and enable practical application, we introduce Environmental Change Detection (ECD). ECD is inspired by real-world practices. To detect changes from past to present, humans first search for relevant images from a past image database. Here, it is an exceptionally rare case to find a perfectly aligned past image. Consequently, the retrieved images may consist entirely of misaligned images with limited field-of-view (FOV) overlap. Under these challenging conditions, humans can detect changes by reconstructing the environment using misaligned past images. We design ECD to reflect these common practices, and a comparison between SCD and ECD is illustrated in Figure 1.

Specifically, ECD shares the same objective as SCD: detecting changes in the query image from the reference. The main distinction is that ECD provides references through a large-scale database without any predefined query-reference pairs. Additionally, a perfectly aligned image may not be included in the database. Consequently, ECD relaxes both assumptions inherent in SCD, making the task more challenging while significantly enhancing its applicability to real-world scenarios.

In addition, we propose a novel framework that jointly understands spatial environments and detects changes. While leveraging the entire reference database could theoretically enhance environmental understanding, this approach incurs significant computational inefficiency. Instead, we retrieve valuable reference candidates that represent the same place in the query image. We then explicitly reconstruct the reference environment oriented to the query image. Here, we deal with the scale variations and misalignments through multi-scale cross-attention mechanisms. This significantly improves the robustness against spatial mismatches. Finally, a change segmentation head is followed.

Moreover, we establish a strong baseline by adapting state-of-the-art methods from related domains to ECD, and reconfigure three standard SCD benchmark sets for ECD. Experimental results highlight the efficacy of our approach and provide constructive insights for future research. Our contributions are summarized as follows:

- We identify practical limitations of the existing SCD task and introduce a new task named ECD.

- We propose the first solution to ECD, achieving comparable performance to the oracle setting.
- We establish standard experimental settings for ECD, providing benchmark datasets and a strong baseline to guide further studies in this area.

2 Related work

Scene change detection. Recent research on scene change detection (SCD) has leveraged deep learning to develop a variety of approaches [12, 13, 14]. DR-TANet [15] introduced the temporal attention module into the encoder-decoder architecture. C-3PO [10] proposes a model that utilizes temporal features to distinguish three types of changes. EMPLACE [3] performs self-supervised learning using a time-interval-based triplet loss. Sachdeva and Zisserman [16] and Lee and Kim [17] utilized synthetic change data. ZSSCD [18] leverages a foundation tracking model to perform change detection without training. Meanwhile, several methods are designed to be robust against misalignment between the reference and query images. SimSac [8] incorporates optical flow estimation and a warping module to account for misalignment. RSCD [11] introduces a cross-attention-based change detection head, enabling comparison even when object positions differ. As such, conventional SCD approaches rely on predefined query-reference pairs. In this work, we avoid these unrealistic assumptions and introduce ECD, a practical problem setting for detecting changes between a query image and a database of uncurated reference images.

Visual place recognition. Visual place recognition (VPR) is the task of estimating the location of a query image by retrieving visually similar images from a pre-collected, geo-tagged database. With the rapid progress of deep learning, numerous effective methods have been proposed to tackle this challenge. NetVLAD [19] is one of the first works to successfully apply deep learning to VPR, outperforming traditional SIFT-based methods [20] and becoming a common baseline in later studies [21, 22, 23, 24, 25]. DINOv2 SALAD [26] reformulates local feature aggregation in VPR as an optimal transport problem using the Sinkhorn algorithm, and employs DINOv2 [27] as the backbone, achieving competitive performance with reduced training cost. BoQ [28] trains learnable global queries that aggregate local features via cross-attention to enable accurate and fast retrieval. Meanwhile, several studies on SCD have been associated with VPR. For example, SimSac [8] utilized VPR to generate a coarsely aligned image pair for SCD. However, ZeroSCD [29] leveraged a VPR backbone for feature extraction in SCD, inspired by the observation that VPR models are inherently robust to variations in style and content. ECD is also closely related to VPR since ground-truths for query-reference pairs and spatial alignments are unavailable. Therefore, VPR can be adopted as a part of the solutions to ECD by generating a noisy query-reference pair.

3 Environmental change detection

3.1 Background: scene change detection (SCD)

Conventional SCD datasets [1, 2, 7] consist of (r, q, y) triplets, where r and q are the pre-change (*i.e.*, reference) and post-change images (*i.e.*, query) taken at time t_0 and t_1 , respectively, and y is the ground-truth change map. The goal is to predict the pixel-wise change mask \hat{y} where the image pair (r, q) is available for every query. This formulation is based on two idealized assumptions: (1) every query image q is paired with a corresponding reference image r , and (2) the pair (r, q) is spatially aligned.

3.2 Problem definition of environmental change detection (ECD)

To address the limitations of SCD and improve real-world applicability, we introduce ECD. ECD relaxes the two unrealistic assumptions of SCD as follows. (1) ECD replaces the availability of the paired reference image with a large-scale reference image database \mathcal{I}_r . This database covers a wide range of environments. Therefore, it is challenging to retrieve useful reference information for a specific query. This setting reflects real-world practices in change detection. (2) In ECD, a perfectly aligned reference image r is not guaranteed for every query q . Practically, it is almost impossible to capture spatially aligned images at different times. Therefore, the reference database is constructed

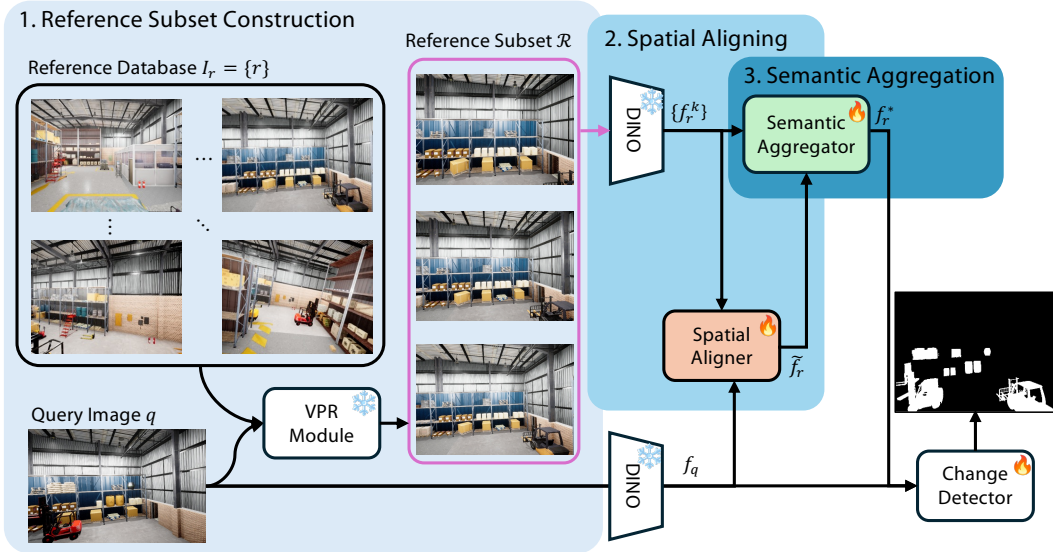


Figure 2: **Overview.** We first construct a subset of the reference database containing images relevant to the query using the VPR module. Then, the spatial aligner focuses on the spatial information of the features to generate a pseudo-aligned view that matches the perspective of the query image. Based on this pseudo-aligned view, the semantic aggregator integrates the semantic information across the subset. Finally, both the reference features and the query features are fed into the change detector to produce the final prediction. In the figure, the snowflake icon represents frozen parameters, and the flame icon represents trainable parameters.

independently of the queries’ FOV while providing sufficient cues for reconstructing the environment. The objective of ECD is to predict a pixel-wise change mask \hat{y} for a given q , based on the reference database \mathcal{I}_r . Note that the reference database \mathcal{I}_r is shared for every query.

4 Method

Figure 2 illustrates the overall architecture of our framework for ECD. We first construct a reference subset by retrieving relevant images from the reference database \mathcal{I}_r . Next, we generate a pseudo-aligned view by spatially aligning features between the subset and the query q . Then, we aggregate semantic features from the subset using the pseudo-aligned view as a spatial anchor. The resulting reference feature, *i.e.*, reconstructed scene, provides a compact and query-aligned summary of the reference database. Finally, change detection is performed using the reconstructed scene and the query.

4.1 Constructing the reference subset

Given the query image q , we construct a reference subset \mathcal{R} from the full reference database \mathcal{I}_r using a pretrained VPR model. The model retrieves the top- K images from \mathcal{I}_r that are estimated to depict the same place as q , based on place-level similarity. These top-ranked images form the reference subset \mathcal{R} :

$$\mathcal{R} = \{r^{(1)}, r^{(2)}, \dots, r^{(K)}\} = \text{TopK}_{\text{VPR}}(q, \mathcal{I}_r), \quad (1)$$

This subset serves as a compact and relevant representation of \mathcal{I}_r for estimating changes with respect to q .

However, in the ECD setting, the query and reference images are taken from different viewpoints. As a result, simply relying on a single top-ranked image may lead to suboptimal performance due to viewpoint misalignment and limited scene coverage. To address these issues, we sequentially perform spatial alignment and semantic aggregation to construct a unified reference representation that resolves both problems. An illustration of the spatial aligner and semantic aggregator is provided in Figure 3.

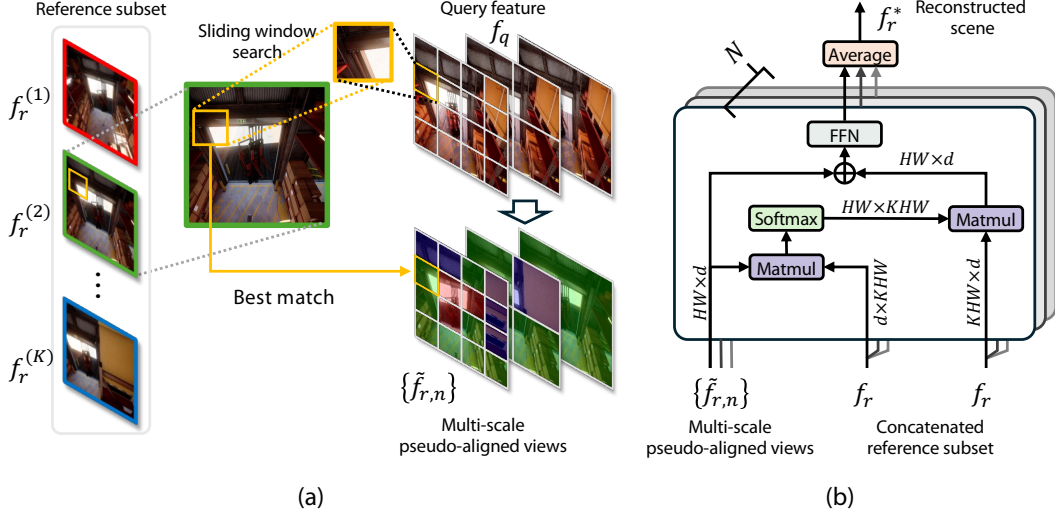


Figure 3: **Illustration of spatial aligner and semantic aggregator.** (a) The input query feature f_q is divided into an $n \times n$ grid. For each grid cell, we perform a sliding window search with stride 1 over all reference features $\{f_r^{(k)}\}_{k=1}^K$ to find the best-matching patch. By collecting the best matches across all grid cells, we construct a pseudo-aligned reference representation $\tilde{f}_{r,n}$ that approximates the viewpoint of the query. This process is performed hierarchically with multiple N scales to capture both coarse and fine-grained correspondences. (b) Features from the reference subset are integrated via cross-attention, using the pseudo-aligned view $\tilde{f}_{r,n}$ as the query. Semantic aggregation is performed at each grid resolution, and the resulting features are averaged to produce the final reconstructed scene f_r^* . Note that the illustration of the multi-head attention (MHA) is omitted for clarity. The N represents the multi-scale of pseudo-aligned views.

4.2 Addressing the spatial mismatch

To address the spatial mismatch between q and $r^{(k)} \in \mathcal{R}$, we introduce the spatial aligner module, which generates a pseudo-aligned view that approximates the geometry of q . All images are initially encoded using a frozen DINO backbone [27] to obtain feature maps f_q and $\{f_r^{(k)}\}_{k=1}^K$. These features are passed through a shared projection head consisting of two convolutional layers with ReLU activations to enhance local contextual representation and similarity discriminability. After then, ℓ_2 -normalized is applied along the feature dimension.

To build the pseudo-aligned view \tilde{f}_r , we divide f_q into an $n \times n$ grid, forming the set of grid locations \mathcal{P}_n . For each grid cell $p \in \mathcal{P}_n$, we extract a patch $f_q[p] \in \mathbb{R}^{d \times h \times w}$, where d , h , and w denote channel, height, and width dimensions, respectively. We compare it to all possible patches from the reference features via sliding window search with stride 1. The patch from any $f_r^{(k)}$ that yields the highest similarity is selected:

$$S_k^p = f_r^{(k)} \otimes f_q[p], \quad \text{for each } k \in [1, K], \quad (2)$$

$$(k^*, z^*) = \arg \max_{k,q} S_k^p[z], \quad (3)$$

where \otimes denotes 2D convolution over spatial dimensions, enabling patch-wise sliding window cosine similarity computation. The corresponding patch is then extracted from the reference map and used to construct the pseudo-aligned feature map:

$$\tilde{f}_{r,n}[p] = f_r^{(k^*)}[z^*]. \quad (4)$$

This process is repeated for all $p \in \mathcal{P}_n$ and across multiple grid resolutions n . Consequently, multi-scale pseudo-aligned views $\{\tilde{f}_{r,n}\}$, which reflects the spatial layout of f_q , are obtained. While the feature $\tilde{f}_{r,n}$ is composed of patches from the reference subset, it is aligned with the query’s FOV, enabling direct matching with the query feature.

4.3 Aggregating the reference features and change segmentation

Each pseudo-aligned view $\tilde{f}_{r,n}$ provides strong spatial alignment with the query feature f_q , but may sacrifice the inherent nature of locality in an image feature because the patches are collected non-locally. Thus, we believe that it has room to enhance the reference representation by integrating semantic features from \mathcal{R} .

To employ this, we introduce a semantic aggregator module that integrates the semantic information contained in \mathcal{R} . We begin by applying a multi-head attention [30] where $\tilde{f}_{r,n}$ is used as the query, and all reference features $\{f_r^{(k)}\}_{k=1}^K$ are concatenated and used as keys and values. The attention output is passed through dropout and combined with the query via a residual connection, followed by a two-layer feed-forward network (FFN) with ReLU activation:

$$f_{r,n}^* = \text{FFN}(\text{Dropout}(\text{MHA}(\tilde{f}_r, f_r, f_r)) + \tilde{f}_r), \quad (5)$$

where $f_r = \text{concat}(f_r^{(1)}, \dots, f_r^{(K)})$.

The resulting representation $f_{r,n}^*$ is semantically enriched and spatially aligned with f_q at grid resolution n . Finally, we generate the reconstructed scene f_r^* by averaging the representations $f_{r,n}^*$. To predict the change, we feed f_r^* and f_q into a change detection module. Following RSCD [11], we adopt a change detection module consisting of a shallow cross-attention block followed by convolutional layers for pixel-level change prediction. The architectural details are provided in the Appendix.

5 Experiments

5.1 Datasets

VL-CMU-CD [1] is a dataset that includes changes in urban street scenes. Following the previous work [11], we resized the image to 504×504 , and split the dataset into 3,324 image pairs for training, 408 pairs for validation, and 429 pairs for testing.

PSCD [2] is a dataset composed of panoramic urban scene images. Following the previous work, we crop each panoramic image into 15 224×224 images. The dataset comprises 9,240 training pairs, 1,155 validation pairs, and 1,155 test pairs. However, PSCD is for testing purposes only, and only evaluations are performed with the best model trained and validated on VL-CMU-CD.

ChangeSim [7] is a synthetic dataset simulating an industrial warehouse environment. It contains 13,225 coarsely aligned image pairs for training and 8,212 for testing. We further split the validation set from the training set, making 8,754 training samples and 4,471 validation samples. Each image is resized to 224×224 . Unlike VL-CMU-CD and PSCD, each image in ChangeSim is sampled from the long sequences. This enables the dataset to provide unaligned reference images, an aspect that has been largely unexplored in prior work. In ECD, we directly utilize the full t_0 sequences as a pre-change database \mathcal{L}_r .

5.2 Implementation details

Reference database. To remove the assumption that a spatially aligned reference image r corresponding to every query q always exists, we sample the original pre-change (*i.e.*, reference) database by applying a database stride s . As a result, the reference database \mathcal{L}_r is downsampled to approximately $1/s$ the size of the original. This effectively makes the benchmark sets more practical and challenging.

Evaluation metrics. Following previous work, we employ the F1-score as the evaluation metric for all datasets.

Training details. Following previous work, we use the Adam optimizer [31] with a learning rate of 1×10^{-4} , and apply a cosine learning rate decay schedule [32]. The model is trained for 100 epochs with a batch size of 4, including 10 warm-up epochs, and using the weighted cross-entropy loss. The VPR model [28] and DINO feature extractor [27] are pre-trained and kept frozen throughout the

Table 1: **Experimental result.** Our method consistently outperforms the baseline across all datasets and database stride s settings.

Database stride	Method	ChangeSim	Dataset VL-CMU-CD	PSCD	Average
1	Oracle	0.3670	0.7950	0.3370	0.4997
	Baseline	0.3688	0.6187	0.2999	0.4291
	Ours	0.3965	0.6941	0.3540	0.4815
3	Baseline	0.3655	0.5485	0.2404	0.3848
	Ours	0.3938	0.5762	0.2667	0.4122
5	Baseline	0.3601	0.4680	0.2027	0.3436
	Ours	0.3906	0.5166	0.2539	0.3870
10	Baseline	0.3545	0.3948	0.2241	0.3245
	Ours	0.3786	0.4355	0.2602	0.3581

pipeline. We constructed the reference subset using the top-3 results from VPR as the default setting, and generated grids for the pseudo-aligned view with resolutions of 1×1 , 2×2 , and 4×4 , which are averaged for final usage.

5.3 Experimental results

We compare our method against a strong baseline that combines state-of-the-art VPR [28] and SCD [11] techniques. Additionally, we report oracle performance, where ground-truth reference images are used during both training and testing, which is equivalent to the standard SCD assumption [11]. As shown in Table 1, our method consistently outperforms the baseline across all datasets and database strides. In the most favorable case, database stride 1, our method achieves an average performance of 0.4815, significantly surpassing the baseline of 0.4291, and approaching the oracle performance of 0.4997.

As the reference database becomes sparser (*i.e.*, as the database stride increases), the overall performance of both the baseline and our method degrades. However, the performance gap between the two remains consistent. These results validate that our feature extraction and compression process enables effective change detection even under significant viewpoint misalignments. Our method not only closes the gap with oracle performance but in some cases, even surpasses it, highlighting its practical utility in real-world deployment scenarios. Notably, on the ChangeSim dataset, where ground-truth pairs are intentionally coarsely aligned, both the baseline and our method outperform the oracle at stride 1. This is because the top-1 reference retrieved by the VPR module at stride 1 is sometimes better aligned with the query than the provided ground-truth pair, resulting in higher accuracy. Beyond this, our method also slightly outperforms the oracle on PSCD, suggesting strong robustness through effective utilization of environmental context, even without perfectly aligned reference images.

We present qualitative results in Figure 4. Here, $r^{(\text{oracle})}$ denotes the ground-truth reference image, which is not included in the reference database but is shown to aid interpretation. The images $r^{(k)}$ are reference images retrieved by the VPR module and are used for prediction. The baseline method is vulnerable to viewpoint differences and often predicts changes at incorrect locations, failing to align properly with the query. In contrast, our method effectively infers spatial context by integrating multiple reference images, enabling more accurate and robust change predictions. These qualitative results demonstrate that our approach performs reliable change detection without requiring a paired and aligned reference image. Additional qualitative examples are provided in the Appendix.

5.4 Ablation study

In Table 2, we perform an ablation study to show the impact of each component in our proposed methods. When the spatial aligner is disabled, feature aggregation is performed using the features from the top-1 VPR result. Conversely, when feature aggregation is disabled, the averaged pseudo-aligned view \tilde{f}_r is directly fed into the change detection module. If both components are removed, features

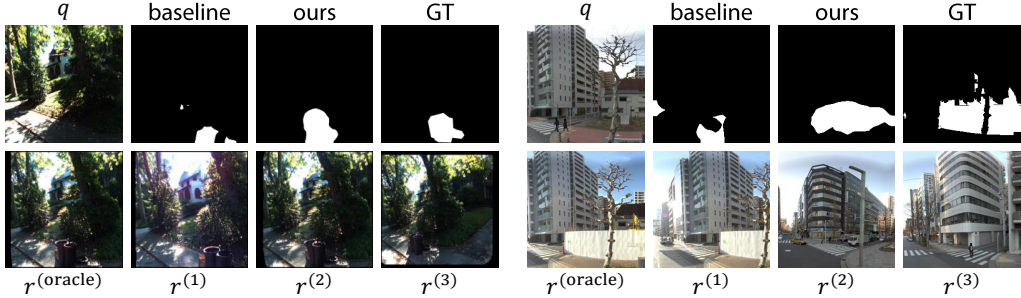


Figure 4: **Qualitative results.** The baseline struggles with viewpoint variation, often predicting changes at incorrect locations. In contrast, our method is more robust to viewpoint mismatch. Note that $r^{(\text{oracle})}$ is not included in the reference database but is shown for illustrative purposes.

Table 2: **Ablation study.** We evaluate the impact of two key components in our method, the semantic aggregator and the spatial aligner. Results across three datasets show that each component individually improves performance, while combining both yields the best results.

Database stride	Method		Dataset			Average
	Agg.	Align	ChangeSim	VL-CMU-CD	PSCD	
1			0.3688	0.6107	0.2999	0.4265
	✓		0.3776	0.6044	0.3280	0.4367
		✓	0.3860	0.6916	0.2827	0.4534
	✓	✓	0.3965	0.6941	0.3540	0.4815
5			0.3601	0.4680	0.2027	0.3436
	✓		0.3574	0.4655	0.2429	0.3553
		✓	0.3734	0.5472	0.2064	0.3757
	✓	✓	0.3906	0.5166	0.2539	0.3870

from the top-1 VPR result are used for change detection, identical to the baseline setup. The results show that both components contribute positively to performance across all datasets. In particular, combining both aggregation and alignment yields the highest average scores, demonstrating their complementary nature.

5.5 Analysis experiments

Number of references images. As shown in Table 3, the performance generally improves as the size of the reference subset K (*i.e.*, the number of reference images) increases, since more reference data provides richer contextual cues. However, we observe performance degradation when K becomes too large, likely due to the inclusion of irrelevant or noisy references. Notably, our method consistently outperforms the baseline even when using only a single reference image, suggesting that the performance gain stems not merely from increased data, but from effective misalignment handling. Considering the trade-off between accuracy and computational efficiency, we set $K = 3$ as the default configuration.

Grid size of the spatial aligner. In Table 4, we study how the choice of grid size in the spatial aligner affects performance. ‘Hier.’ denotes a hierarchical configuration: hierarchical $\times 2$ averages representations obtained from 1×1 and 2×2 grids, while hierarchical $\times 3$ additionally incorporates a 4×4 grid level. We observe that hierarchical configurations consistently outperform fixed single-scale grids, with hierarchical $\times 3$ achieving the highest average performance across both dataset stride settings.

Table 3: **Analysis experiment on the size of the reference subset.** The performance tends to improve as the size of the reference subset K increases, but degrades when too many references are used.

Database stride	K	ChangeSim	Dataset VL-CMU-CD	PSCD	Average
1	Baseline	0.3688	0.6107	0.2999	0.4265
	1	0.3837	0.6281	0.3209	0.4442
	3	0.3965	0.6941	0.3540	0.4815
	5	0.3897	0.7258	0.3458	0.4871
	10	0.3987	0.7045	0.3387	0.4806
5	Baseline	0.3601	0.4680	0.2027	0.3436
	1	0.3790	0.5099	0.2398	0.3762
	3	0.3906	0.5166	0.2539	0.3870
	5	0.3908	0.5085	0.2566	0.3853
	10	0.3816	0.5571	0.1972	0.3786

Table 4: **Analysis experiment on the grid size of the spatial aligner.** ‘Hier.’ is an abbreviation for *hierarchical*. Hierarchical settings generally show improved performance, with ‘Hier. $\times 3$ ’ achieving the best result.

Database stride	Grid size	ChangeSim	Dataset VL-CMU-CD	PSCD	Average
1	Baseline	0.3688	0.6187	0.2999	0.4291
	1 \times 1	0.3751	0.6810	0.3418	0.4660
	2 \times 2	0.3891	0.6805	0.2818	0.4505
	4 \times 4	0.3928	0.6314	0.2543	0.4262
	Hier. $\times 2$	0.3814	0.6971	0.3381	0.4722
	Hier. $\times 3$ (Ours)	0.3965	0.6941	0.3540	0.4815
5	Baseline	0.3601	0.4680	0.2027	0.3436
	1 \times 1	0.3740	0.4689	0.2262	0.3564
	2 \times 2	0.3815	0.4768	0.1964	0.3516
	4 \times 4	0.3867	0.4252	0.2218	0.3446
	Hier. $\times 2$	0.3849	0.5013	0.2466	0.3776
	Hier. $\times 3$ (Ours)	0.3906	0.5166	0.2539	0.3870

6 Limitations

To formulate practical problems, ECD does not utilize query-reference pairs. Nevertheless, the reference database must include FOV overlaps with queries to enable change detection. Additionally, this problem setting increases the computational burden of the framework. Unlike conventional SCD methods that utilize ground-truth image pairs, our framework identifies reference candidates via a VPR step. These limitations remain open challenges for developing more practical solutions.

7 Conclusion

In this paper, we introduced a new task termed environmental change detection (ECD), which removes two unrealistic assumptions commonly made in conventional scene change detection (SCD) settings: the presence of a predefined reference-query pair and the availability of a perfectly aligned reference image for every query. ECD is a more challenging and realistic problem setting that better reflects real-world scenarios. In addition, we also propose a novel solution to ECD. Rather than relying on the entire reference database, we first construct a reference subset by retrieving relevant images from a large-scale reference database. We then apply spatial alignment and semantic aggregation to reconstruct the scene corresponding to the query viewpoint from the database. The resulting reference scene preserves rich environmental information of the reference database and aligns well with the query view, providing a reliable foundation for ECD. Our method outperforms a strong baseline

composed of state-of-the-art VPR and SCD models, demonstrating its ability to handle misalignment more effectively. We believe this work moves change detection closer to practical deployment by enabling robust performance in less constrained, more realistic scenarios.

References

- [1] Pablo F Alcantarilla, Simon Stent, German Ros, Roberto Arroyo, and Riccardo Gherardi. Street-view change detection with deconvolutional networks. *Autonomous Robots*, 42:1301–1322, 2018.
- [2] Ken Sakurada, Mikiya Shibuya, and Weimin Wang. Weakly supervised silhouette-based semantic scene change detection. In *2020 IEEE International conference on robotics and automation (ICRA)*, pages 6861–6867. IEEE, 2020.
- [3] Tim Alpherts, Sennay Ghebreab, and Nanne van Noord. Emplace: Self-supervised urban scene change detection. In *Proceedings of the AAAI Conference on Artificial Intelligence*, volume 39, pages 1737–1745, 2025.
- [4] Ken Sakurada and Takayuki Okatani. Change detection from a street image pair using cnn features and superpixel segmentation. In *British Machine Vision Conference (BMVC)*, 2015.
- [5] Kyeongjin Ahn, Sungwon Han, Sungwon Park, Jihee Kim, Sangyoon Park, and Meeyoung Cha. Generalizable disaster damage assessment via change detection with vision foundation model. In *Proceedings of the AAAI Conference on Artificial Intelligence*, volume 39, pages 27784–27792, 2025.
- [6] Dong Li, Lineng Chen, Cheng-Zhong Xu, and Hui Kong. Umad: University of macau anomaly detection benchmark dataset. In *2024 IEEE/RSJ International Conference on Intelligent Robots and Systems (IROS)*, pages 5836–5843. IEEE, 2024.
- [7] Jin-Man Park, Jae-Hyuk Jang, Sahng-Min Yoo, Sun-Kyung Lee, Ue-Hwan Kim, and Jong-Hwan Kim. Changesim: Towards end-to-end online scene change detection in industrial indoor environments. In *2021 IEEE/RSJ International Conference on Intelligent Robots and Systems (IROS)*, pages 8578–8585. IEEE, 2021.
- [8] Jin-Man Park, Ue-Hwan Kim, Seon-Hoon Lee, and Jong-Hwan Kim. Dual task learning by leveraging both dense correspondence and mis-correspondence for robust change detection with imperfect matches. In *Proceedings of the IEEE/CVF Conference on Computer Vision and Pattern Recognition (CVPR)*, pages 13749–13759, 2022.
- [9] Yinjie Lei, Duo Peng, Pingping Zhang, QiuHong Ke, and Haifeng Li. Hierarchical paired channel fusion network for street scene change detection. *IEEE Transactions on Image Processing*, 30:55–67, 2020.
- [10] Guo-Hua Wang, Bin-Bin Gao, and Chengjie Wang. How to reduce change detection to semantic segmentation. *Pattern Recognition*, 138:109384, 2023.
- [11] Chun-Jung Lin, Sourav Garg, Tat-Jun Chin, and Feras Dayoub. Robust scene change detection using visual foundation models and cross-attention mechanisms. *arXiv preprint arXiv:2409.16850*, 2024.
- [12] Vijaya Raghavan T Ramkumar, Prashant Bhat, Elahe Arani, and Bahram Zonooz. Self-supervised pretraining for scene change detection. In *Proceedings of the 35th Conference on Neural Information Processing Systems*, pages 6–14, 2021.
- [13] Ragav Sachdeva and Andrew Zisserman. The change you want to see. In *Proceedings of the IEEE/CVF Winter Conference on Applications of Computer Vision*, pages 3993–4002, 2023.
- [14] Seonhoon Lee and Jong-Hwan Kim. Semi-supervised scene change detection by distillation from feature-metric alignment. In *Proceedings of the IEEE/CVF Winter Conference on Applications of Computer Vision (WACV)*, pages 1226–1235, 2024.

- [15] Shuo Chen, Kailun Yang, and Rainer Stiefelhagen. Dr-tanet: Dynamic receptive temporal attention network for street scene change detection. In *2021 IEEE Intelligent Vehicles Symposium (IV)*, pages 502–509. IEEE, 2021.
- [16] Ragav Sachdeva and Andrew Zisserman. The change you want to see. In *Proceedings of the IEEE/CVF Winter Conference on Applications of Computer Vision (WACV)*, 2023.
- [17] Seonhoon Lee and Jong-Hwan Kim. Semi-supervised scene change detection by distillation from feature-metric alignment. In *Proceedings of the IEEE/CVF Winter Conference on Applications of Computer Vision (WACV)*, pages 1226–1235, January 2024.
- [18] Kyusik Cho, Dong Yeop Kim, and Euntai Kim. Zero-shot scene change detection. In *Proceedings of the AAAI Conference on Artificial Intelligence*, volume 39, pages 2509–2517, 2025.
- [19] Relja Arandjelovic, Petr Gronat, Akihiko Torii, Tomas Pajdla, and Josef Sivic. Netvlad: Cnn architecture for weakly supervised place recognition. In *Proceedings of the IEEE Conference on Computer Vision and Pattern Recognition (CVPR)*, pages 5297–5307, 2016.
- [20] David G Lowe. Object recognition from local scale-invariant features. In *Proceedings of the seventh IEEE international conference on computer vision*, volume 2, pages 1150–1157. Ieee, 1999.
- [21] Qibo Qiu, Shun Zhang, Haiming Gao, Honghui Yang, Haochao Ying, Wenxiao Wang, and Xiaofei He. Emvp: Embracing visual foundation model for visual place recognition with centroid-free probing. *Advances in Neural Information Processing Systems*, 37:120928–120950, 2024.
- [22] Feng Lu, Xinyao Zhang, Canming Ye, Shuting Dong, Lijun Zhang, Xiangyuan Lan, and Chun Yuan. Supervlad: Compact and robust image descriptors for visual place recognition. *Advances in Neural Information Processing Systems*, 37:5789–5816, 2024.
- [23] Sijie Zhu, Linjie Yang, Chen Chen, Mubarak Shah, Xiaohui Shen, and Heng Wang. R2former: Unified retrieval and reranking transformer for place recognition. In *Proceedings of the IEEE/CVF Conference on Computer Vision and Pattern Recognition (CVPR)*, pages 19370–19380, 2023.
- [24] Ruotong Wang, Yanqing Shen, Weiliang Zuo, Sanping Zhou, and Nanning Zheng. Transvpr: Transformer-based place recognition with multi-level attention aggregation. In *Proceedings of the IEEE/CVF Conference on Computer Vision and Pattern Recognition (CVPR)*, pages 13648–13657, 2022.
- [25] Feng Lu, Xiangyuan Lan, Lijun Zhang, Dongmei Jiang, Yaowei Wang, and Chun Yuan. Cricavpr: Cross-image correlation-aware representation learning for visual place recognition. In *Proceedings of the IEEE/CVF Conference on Computer Vision and Pattern Recognition (CVPR)*, pages 16772–16782, 2024.
- [26] Sergio Izquierdo and Javier Civera. Optimal transport aggregation for visual place recognition. In *Proceedings of the IEEE/CVF Conference on Computer Vision and Pattern Recognition (CVPR)*, pages 17658–17668, 2024.
- [27] Maxime Oquab, Timothée Darcet, Théo Moutakanni, Huy Vo, Marc Szafraniec, Vasil Khalidov, Pierre Fernandez, Daniel Haziza, Francisco Massa, Alaaeldin El-Nouby, et al. Dinov2: Learning robust visual features without supervision. *arXiv preprint arXiv:2304.07193*, 2023.
- [28] Amar Ali-Bey, Brahim Chaib-draa, and Philippe Giguère. Boq: A place is worth a bag of learnable queries. In *Proceedings of the IEEE/CVF Conference on Computer Vision and Pattern Recognition*, pages 17794–17803, 2024.
- [29] Shyam Sundar Kannan and Byung-Cheol Min. Zeroscd: Zero-shot street scene change detection. *arXiv preprint arXiv:2409.15255*, 2024.

- [30] Ashish Vaswani, Noam Shazeer, Niki Parmar, Jakob Uszkoreit, Llion Jones, Aidan N Gomez, Łukasz Kaiser, and Illia Polosukhin. Attention is all you need. *Advances in neural information processing systems*, 30, 2017.
- [31] Diederik P. Kingma and Jimmy Ba. Adam: A method for stochastic optimization. In *International Conference for Learning Representations*, 2015.
- [32] Ilya Loshchilov and Frank Hutter. Sgdr: Stochastic gradient descent with warm restarts. In *International Conference for Learning Representations*, 2017.
- [33] Kaiming He, Xiangyu Zhang, Shaoqing Ren, and Jian Sun. Deep residual learning for image recognition. In *Proceedings of the IEEE conference on computer vision and pattern recognition*, pages 770–778, 2016.
- [34] Noé Pion, Martin Humenberger, Gabriela Csurka, Yohann Cabon, and Torsten Sattler. Benchmarking image retrieval for visual localization. In *2020 International Conference on 3D Vision (3DV)*, pages 483–494. IEEE, 2020.

A Implementation details

A.1 Details on ECD setup preparation

We describe the detailed procedure for preparing the experimental setup used in ECD. Starting from the standard SCD datasets, which consist of triplets (r, q, y) , we first collect all reference images r and build the database. The query images q and their corresponding labels y are used without modification from the SCD setup. To remove the assumption that a spatially aligned reference image r always exists for every query q , we restrict the size of the database by applying a database stride s . Specifically, only every s -th image in the sequence from the original database is included in the reference database \mathcal{I}_r .

Given that several SCD datasets (*e.g.*, VL-CMU-CD [1] and ChangeSim [7]) are composed of multiple sequences, we apply the stride on a per-sequence basis. Thus, only every s -th image within each sequence is included in the reference database \mathcal{I}_r . For PSCD [2], where each panorama image is divided into 15 crops, we treat the set of cropped images from a single panorama as a sequence and apply the stride accordingly.

Formally, \mathcal{I}_r is defined as:

$$\mathcal{I}_r = \left\{ r^{(m,j)} \mid j \in \{1, 1 + s, 1 + 2s, \dots\}, j \leq L_m \text{ for each sequence } m \right\}, \quad (6)$$

where L_m denotes the length of sequence m . This striding constraint reduces the spatial and temporal coverage of the reference database and removes the guarantee that a ground-truth reference-query pair exists.

The examples of the original and strided reference database are illustrated in Figure 5. As shown in the figure, applying a stride naturally sparsifies the reference set, limiting the spatial extent each query can be matched to and making reliable retrieval more challenging. The viewpoint difference between images varies significantly across datasets, realistically reflecting the fact that viewpoint coverage in the database is unknown in real-world scenarios.

A.2 Details on architecture

VPR module. We use a pre-trained BoQ model [28] without any architectural modifications. The feature extractor in BoQ is pre-trained ResNet-50 [33].

Spatial aligner. For feature extraction from both r and q , we use the DINOv2-ViT-S/14 model [27]. Extracted features are passed through a projection head before similarity computation. The projection head consists of two 5×5 convolutions with ReLU activation function.

Semantic aggregator. We use multi-head attention with 6 heads and a dropout rate of 0.1. The feed-forward network (FFN) following the attention layer consists of 384 dimensions.

Change detection head. The change detection head operates on the extracted feature from the reference database, the reconstructed scene f_r^* , and the query feature f_q . Its architecture is identical to the PSCD [11]. First, two cross-attentions are applied in both directions from f_r^* to extract information corresponding to f_q , and vice versa. The resulting features are concatenated and passed through a sequence of layers: a 3×3 convolution that reduces the number of channels by half, followed by a 1×1 convolution to produce a single-channel change prediction map, and finally an upsampling layer. This yields the final change detection output. This yields the final change prediction output.

A.3 Experiments compute resources

The experiments were performed on a system with the Intel Xeon Gold 6426Y CPU and a single NVIDIA RTX A5000 GPU. The software environment comprised Python 3.10.16 and PyTorch 2.1.0, with CUDA version 12.2. The total GPU memory usage during the experiments remained below 24 GB. Training takes approximately 5 hours on the ChangeSim dataset and 10 hours on VL-CMU-CD. PSCD is a test-only dataset and is not involved in training.

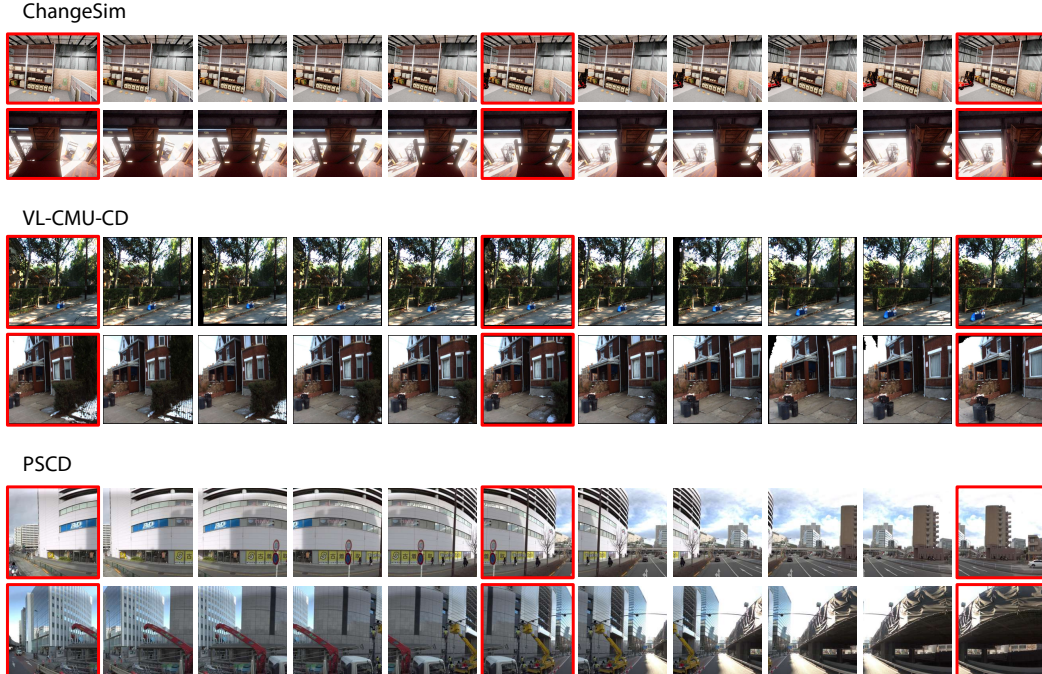


Figure 5: **Example images from the reference database.** The figure compares the full reference database used in the conventional SCD setting with the strided reference database in the proposed ECD setup. The images outlined in red boxes represent the reference images selected for the ECD reference database, using a database stride setting of $s = 5$. By applying a stride, ECD reduces the spatial and temporal density of the reference set, thereby intentionally introducing misalignment between queries and available references. Best viewed when zoomed in.

B VPR results

We evaluate the top-1 retrieval accuracy of the VPR module to assess how effectively it retrieves relevant reference images under varying database stride values. To facilitate this analysis, we define two levels of matching criteria: *strict match* and *coarse match*, with results presented in Table 5. Note that these criteria are used exclusively for analysis in this section and are not incorporated into the main pipeline.

A *strict match* is defined as follows: for VL-CMU-CD and PSCD, it corresponds to the exact ground-truth reference pair; for ChangeSim, it refers to retrieved images within 1 meter and 10 degrees of the query, following SimSac [8], which only considers distance. A *coarse match* is defined more loosely: for VL-CMU-CD and PSCD, it includes any image from the same sequence as the ground-truth; for ChangeSim, it refers to retrieved images within 25 meters and 45 degrees of the query, following the retrieval metric [34].

As the stride increases, the retrieval accuracy for strict matches drops sharply, whereas coarse match rates remain relatively stable. This indicates that strictly relying on GT-aligned references becomes increasingly impractical at larger strides. Instead, models must leverage nearby images to support accurate predictions. Interestingly, for VL-CMU-CD, the top-1 retrieval accuracy is lower compared to other datasets. This is because there is minimal viewpoint variation within each sequence, making many reference images visually similar and difficult to distinguish.

C Qualitative visualizations of the spatial aligner

We provide visual examples in Figures 6, 7, and 8 to showcase the effectiveness of our proposed spatial aligner in producing hierarchical pseudo-aligned views. In the visual examples, q denotes the query image, $r^{(\text{oracle})}$ is the ground truth reference image, and $r^{(k)} \in \mathcal{R}$ are the top- K retrievals from

Table 5: **The accuracy of the VPR module.** Each value is the average accuracy (%) computed on the training, validation, and test splits.

Database stride	ChangeSim		VL-CMU-CD		PSCD		Avg. (Strict)	Avg. (Coarse)
	Strict	Coarse	Strict	Coarse	Strict	Coarse		
1	53.17	99.21	32.59	84.45	93.08	97.90	59.61	93.85
3	51.64	99.10	23.27	84.39	32.51	96.98	35.81	93.49
5	47.96	99.01	18.64	84.13	19.86	88.04	28.82	90.40
10	42.02	98.10	12.65	83.74	13.28	68.29	22.65	83.38

the reference database \mathcal{I}_r . Note that $r^{(\text{oracle})}$ is not guaranteed to be included in the reference database depending on the query and database stride, but is shown here for illustrative purposes. The retrieved reference images are visually marked as follows: green borders indicate a strict match, blue borders indicate a coarse match, and red borders indicate incorrect matches.

The spatial aligner operates on features, and the resulting pseudo-aligned views $\tilde{f}_{r,n}$ are also feature representations. Therefore, these are visualized as images using the coordinates of the matched patches. The notation $\tilde{f}_{r,n}$ represents the pseudo-aligned view generated with an $n \times n$ grid. For improved visibility, we also provide a colored version in which the color indicates the origin of each patch from the reference images. Specifically, $r^{(1)}$, $r^{(2)}$, and $r^{(3)}$ are colored in cyan, magenta, and yellow, respectively. To aid in understanding viewpoint alignment, potential keypoints are highlighted with black or orange boxes.

Figure 6 presents examples of pseudo-aligned views. It shows that our method can successfully imitate query views by selecting high-similarity patches for each query patch from multiple reference images. In particular, the pseudo-aligned views on the 4×4 grid effectively approximate the target viewpoints.

Figure 7 illustrates a scenario involving changes of the large object. Because the spatial aligner operates at the patch-level similarity, alignment accuracy may degrade at finer grid resolutions, especially when a patch is entirely altered. Despite this, the hierarchical structure of the aligner ensures robustness at coarser grid resolutions, effectively handling large changes and substantial scene variations. These results highlight the complementary roles of fine- and coarse-level alignment, validating our hierarchical design.

Figure 8 depicts a challenging case with a large database stride s , where no correctly aligned reference images are available. Even under these conditions, the spatial aligner effectively suppresses the influence of unrelated images and reconstructs the view primarily using the relevant match.

These results provide strong evidence that the proposed spatial aligner can operate effectively. However, since the outputs may exhibit semantic inconsistencies, particularly around patch boundaries, they serve as better feature representations when used in conjunction with the proposed semantic aggregator.

D Additional qualitative results

We present additional qualitative results across various datasets in Figures 9, 10, and 11. We provide prediction results for each query image q under two different dataset stride s settings, to illustrate how spatial information and prediction difficulty vary depending on the sparsity of the reference database.

As in the previous section, $r^{(\text{oracle})}$ is the ground truth reference image, and $r^{(k)} \in \mathcal{R}$ are the retrieved reference subset \mathcal{R} . The borders of the reference images are colored to indicate match quality: green for strict matches, blue for coarse matches, and red for incorrect matches.

Our method achieves accurate predictions even without exact viewpoint matches by leveraging nearby frames. Moreover, it demonstrates greater robustness to viewpoint changes compared to the baseline. Even when the VPR retrieval includes incorrect matches, most notably observed in the PSCD dataset under the $s = 5$ setting, our model can still produce accurate predictions, thanks to effective attention mechanisms.

E Broader impacts

SCD and the proposed ECD can be applied to a wide range of real-world scenarios, including natural disaster assessment, urban development monitoring, and automated warehouse management. These technologies have the potential to enhance safety, efficiency, and environmental awareness. However, their deployment also raises privacy violations or surveillance applications. Care must be taken to ensure that such systems are developed and used in a way that respects individual rights and complies with legal and ethical standards.

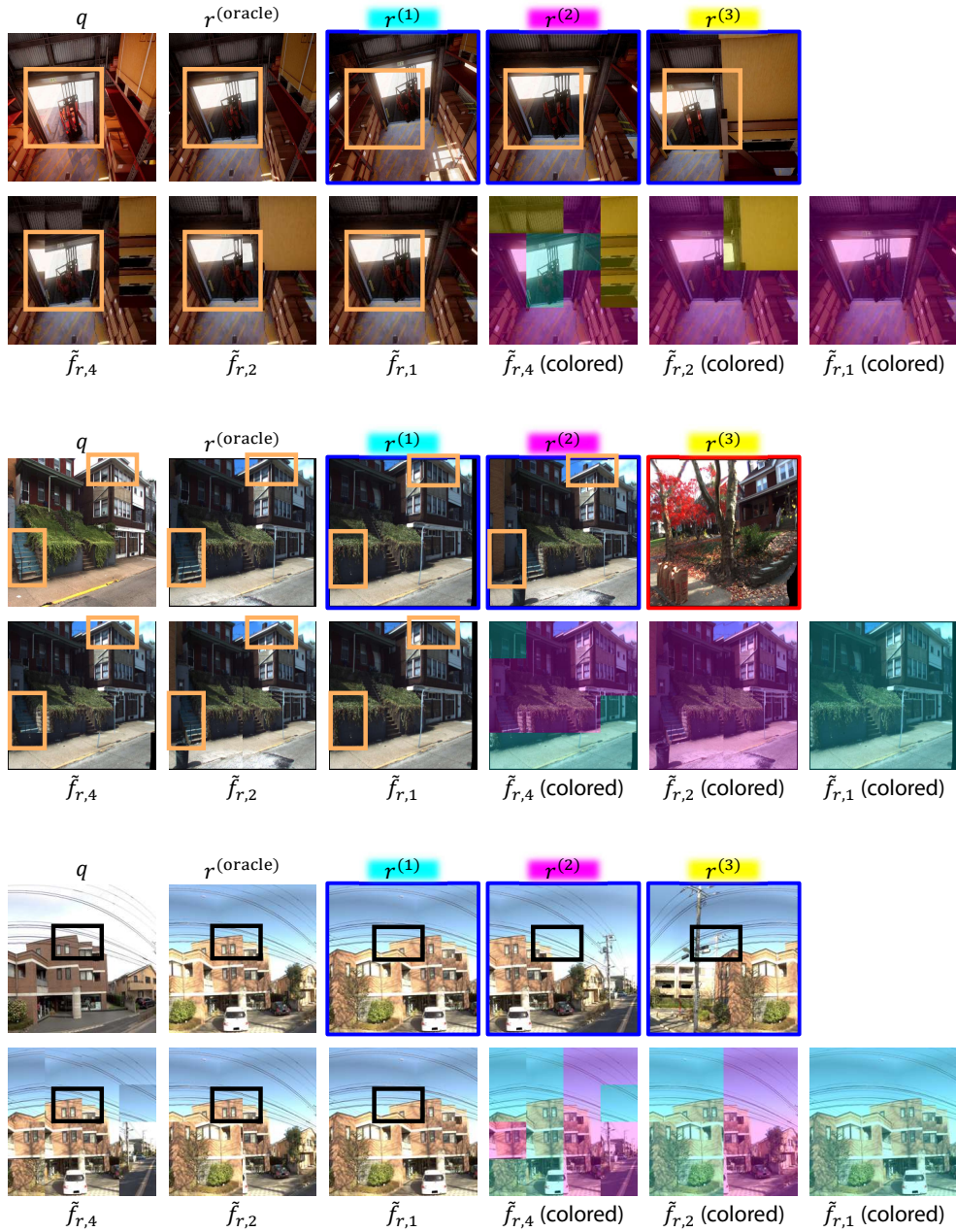


Figure 6: **Examples of pseudo-aligned views.** Given a query image q , the spatial aligner generates pseudo-aligned views at multiple grid levels using reference images $r^{(1)}$, $r^{(2)}$, and $r^{(3)}$. $r^{(\text{oracle})}$ is shown for reference purposes. At finer grid levels, the generated views closely imitate the viewpoint of the query. The borders of the reference images are colored to indicate match quality: green for strict matches, blue for coarse matches, and red for incorrect matches.

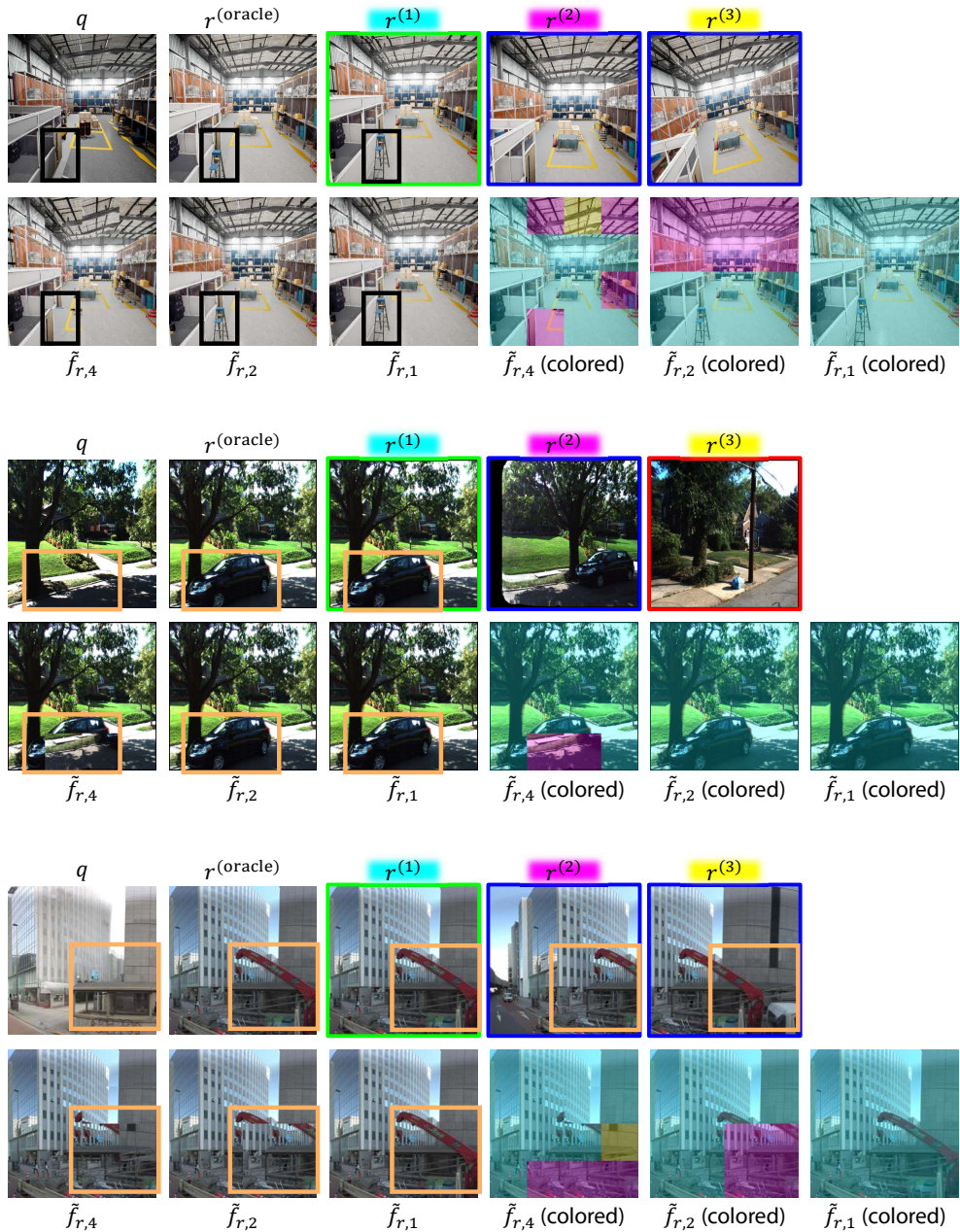


Figure 7: **Examples of pseudo-aligned views under large object changes.** When a substantial change spans the entire area of a patch, the pseudo-aligned view at fine grid levels may fail to align accurately. However, the pseudo-aligned view at fine grid levels works robustly, provides strong evidence for the effectiveness of the hierarchical approach.

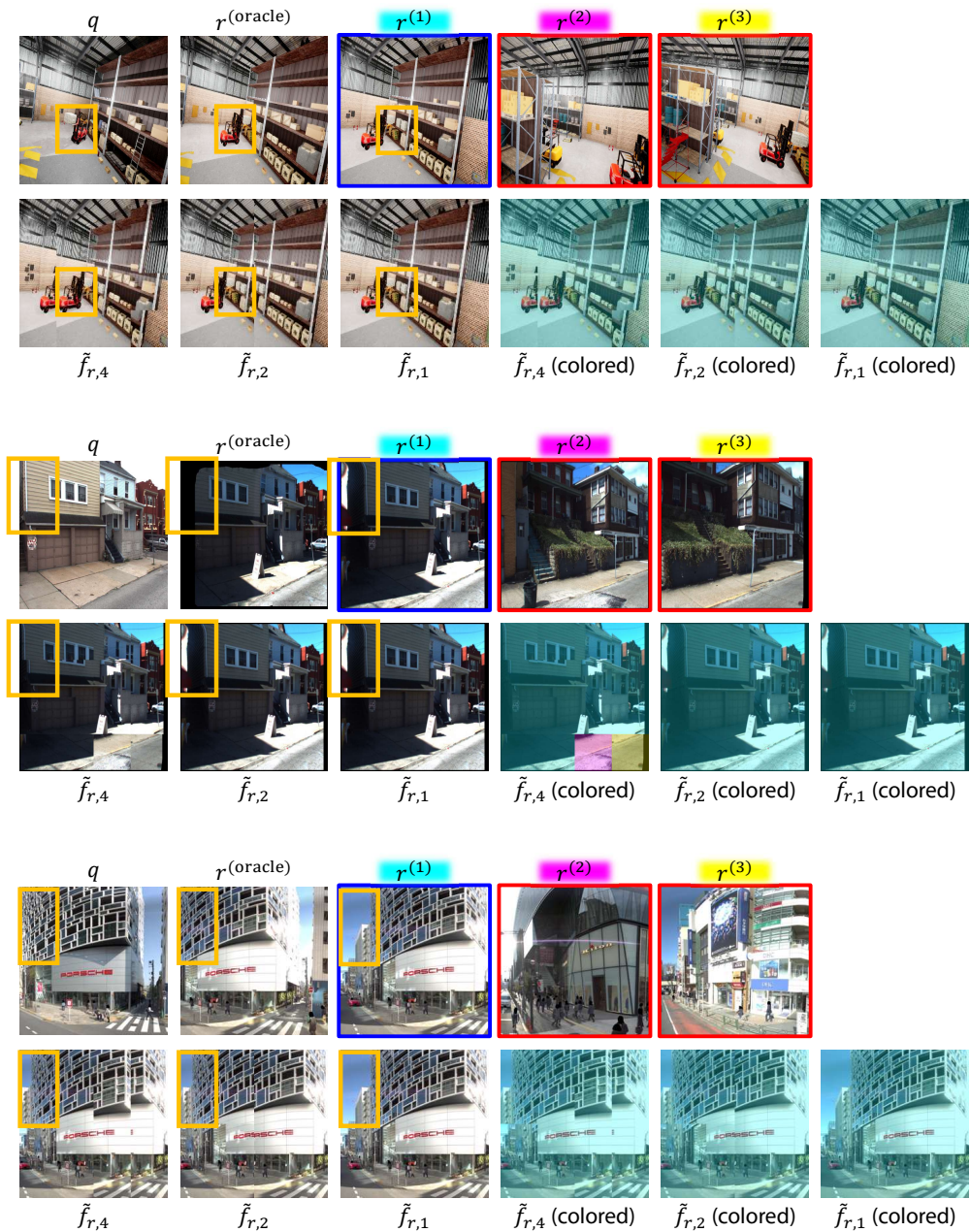


Figure 8: **Examples of pseudo-aligned views under a large database stride.** Even when the reference subset \mathcal{R} contains many incorrect reference images, the spatial aligner effectively suppresses the influence of unrelated images and reconstructs the pseudo-aligned view primarily using the most relevant match.

ChangeSim

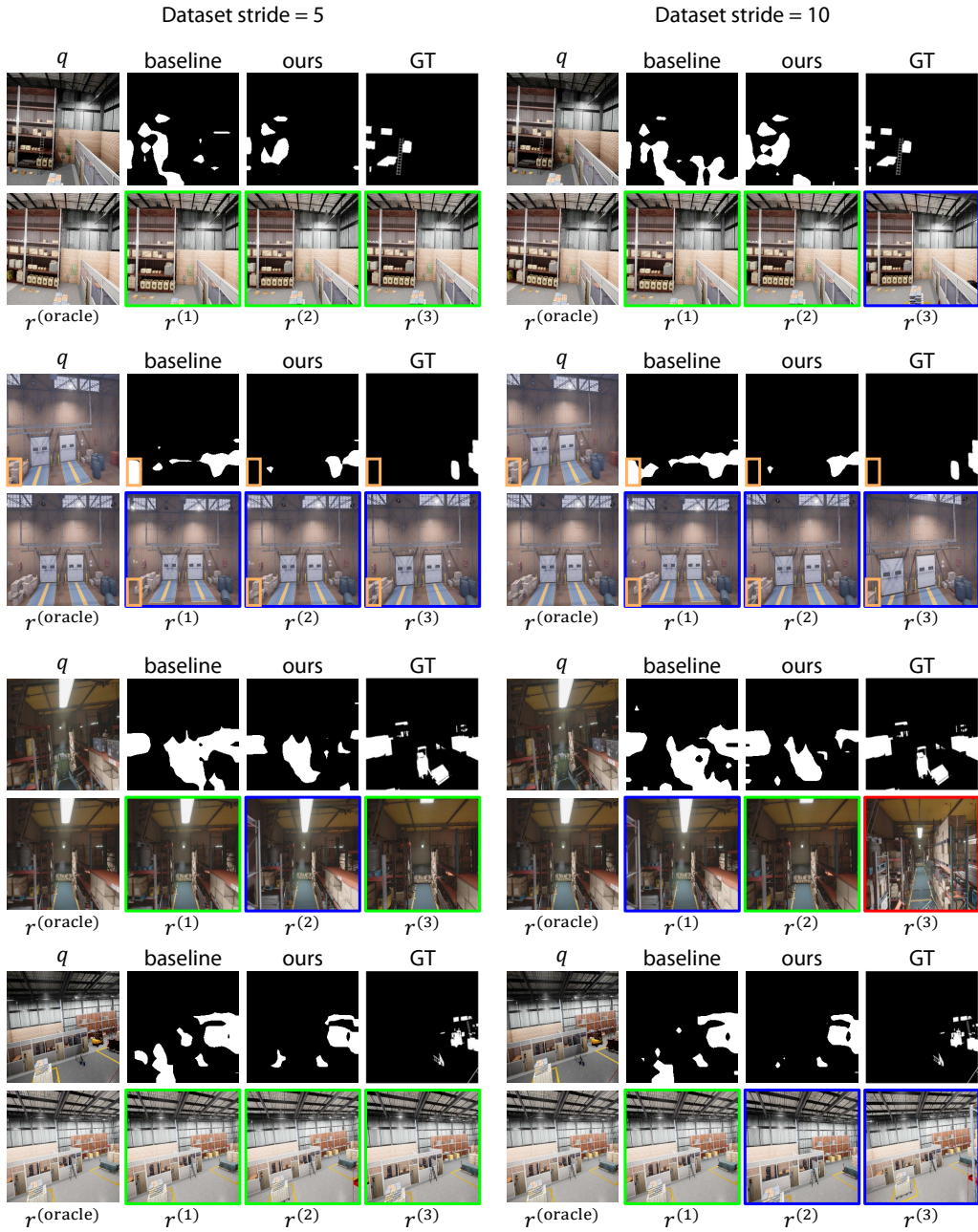


Figure 9: **Qualitative results on ChangeSim.** Our method performs robust predictions even in complex scenes by effectively integrating spatial information.

VL-CMU-CD

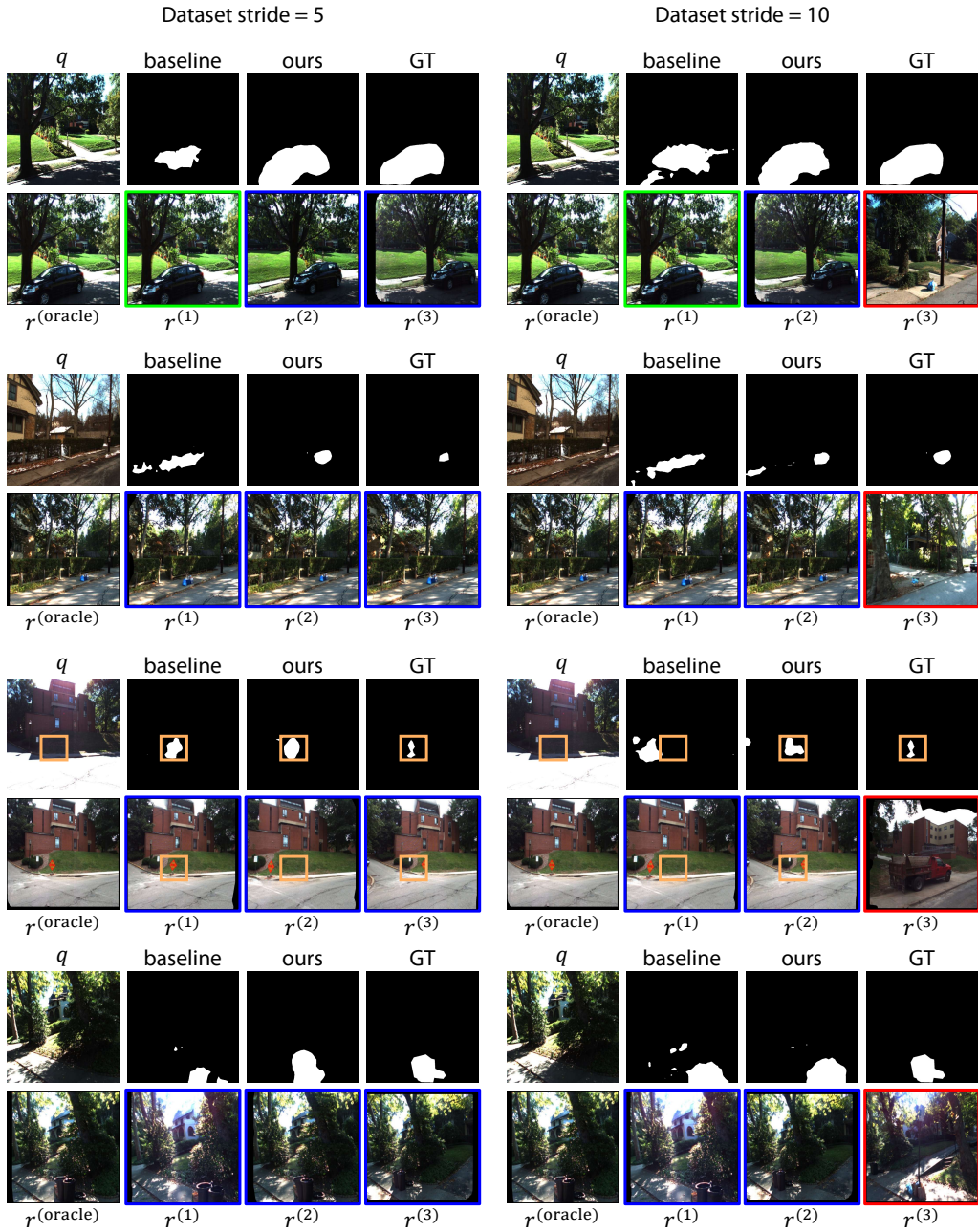


Figure 10: **Qualitative results on VL-CMU-CD.** Our method is more robust to viewpoint variations than the baseline.

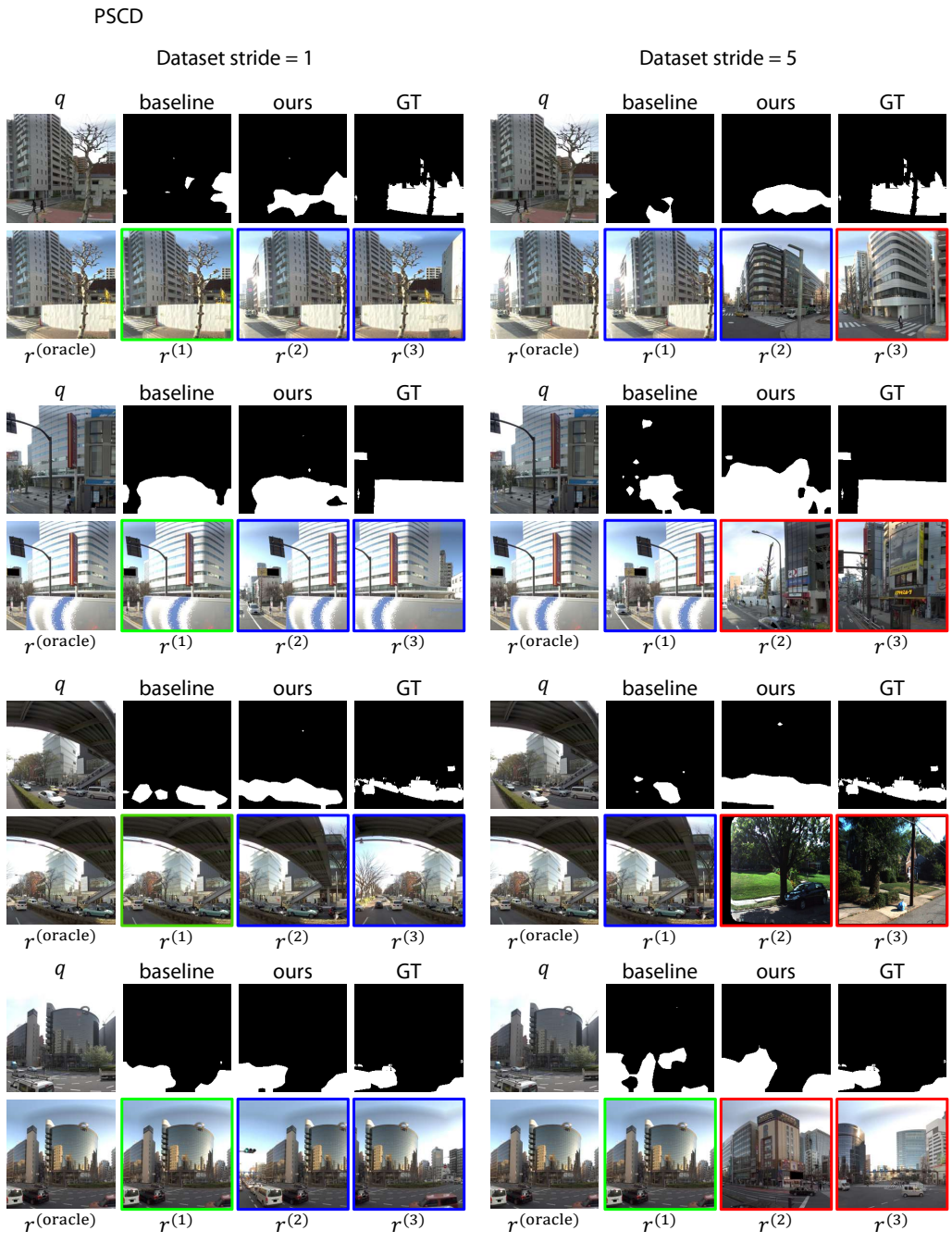


Figure 11: **Qualitative results on PSCD.** Even when the VPR retrieval includes incorrect matches, our model can still produce accurate predictions.